INC-40007-137

Heating ^{197}Au Nuclei with 8 GeV Antiproton and π^- Beams*

T. Lefort, K. Kwiatkowski[1], V.E. Viola, W.-c. Hsi, and L. Beaulieu
Department of Chemistry and IUCF, Indiana University, Bloomington, IN 47405

L. Pienkowski
Heavy Ion Laboratory, Warsaw University, Warsaw Poland

R.G. Korteling
Department of Chemistry, Simon Fraser University, Burnaby, B.C., V5A 1S6 Canada

R. Laforest, E. Martin, E. Ramakrishnan,
D. Rowland, A. Ruangma, E. Winchester and S.J. Yennello
Department of Chemistry and Cyclotron Lab, Texas A & M University, College Station, TX 77843

S. Gushue and L.P. Remsberg
Physics Division, Brookhaven National Laboratory, Upton, NY 11973

H. Breuer
Department of Physics, University of Maryland, College Park, MD 20740

B. Back
Physics Division, Argonne National Laboratory, 9700 S. Cass Avenue, Argonne, IL 60439

[to be published in *Proceedings of the XXXVII International Winter Meeting on Nuclear Physics,* Bormio, Italy, Jan. 25-30, 1999]

*Research supported by the U.S. Department of Energy and National Science Foundation, the National Sciences and Engineering Research Council of Canada, the Robert A. Welch Foundation and Grant No. P03B 048 15 of the Polish State Committee for Scientific Research.

[1]Present address: Los Alamos National Laboratory, Los Alamos, NM 87545

DISCLAIMER

DISCLAIMER

Portions of this document may be illegible in electronic image products. Images are produced from the best available original document.

Heating ^{197}Au Nuclei with 8 GeV/c Antiproton and π^- Beams

T. Lefort[1], K. Kwiatkowski[1,2], W.-c. Hsi,[1], L. Pienkowski[3], L. Beaulieu[1], B. Back[4], H. Breuer[5], S. Gushue[6], R.G. Korteling[7], R. Laforest[8], E. Martin[8], E. Ramakrishnan[8], L.P. Remsberg[6], D. Rowland[8], A. Ruangma[8], V.E. Viola[1], E. Winchester[8], S.J. Yennello[8]

[1]Department of Chemistry and IUCF, Indiana University Bloomington, IN 47405
[2]Los Alamos National Laboratory, Los Alamos, NM 87545
[3]Heavy Ion Laboratory, Warsaw University, 02 097 Warsaw Poland
[4]Physics Division, Argonne National Laboratory, 9700 S. Cass Ave., Argonne, IL 60439
[5]Department of Physics, University of Maryland, College Park, MD 20742
[6]Physics Divsion, Brookhaven National Laboratory, Upton, NY 11973
[7]Department of Chemistry, Simon Fraser University, Burnaby, B.C., V5A 1S6 Canada
[8]Department of Chemistry and Cyclotron Laboratory, Texas A&M University, College Station, TX 77843, U.S.A.

Abstract

This contribution stresses results recently obtained from experiment E900 performed at the Brookhaven AGS accelerator with 8 GeV/c antiproton and negative pion beams using the Indiana Silicon Sphere detector array. An investigation of the reaction mechanism is presented, along with source characteristics deduced from a two-component fit to the spectra. An enhancement of deposition energy with the antiproton beam with respect to the pion beam is observed. The results are qualitatively consistent with predictions of an intranuclear cascade code.

1 Introduction

Collisions between GeV light projectiles (π, p, $\bar{\text{p}}$,^{3}He, etc ...) on heavy target nuclei create highly excited nuclei with weak collective excitations due to compression, rotation and/or shape distortion [1]. The rapid thermalization ($\approx$ 30 fm/c [2]) achieved in the target-like residue formed in such reactions allows one to study the decay of highly excited nuclei, especially the thermal multifragmentation channel[3, 4]. Due to the trapping of at least part of the annihilation energy in the heavy residue, antiproton beams are expected to enhance the energy deposition with respect to the other hadron beams, enabling a broader energy-deposition range to be studied.

The reaction mechanism is usually understood and modeled in two steps. During the first $\approx$ 30 fm/c a cascade of pions and nucleons, induced by the initial interaction between the light projectile and target nucleons, evolves in the target nucleus. Then, the deexcitation of the heavy-residual nucleus takes place. The energy deposition occurs during the cascade via a succession of elastic and/or inelastic (π,N)-N collisions and pion

absorption (Δ, N^* resonances). Some of the hadrons involved in the cascade escape from the target nucleus and contribute to the nonequilibrium emission of light charged particles, as well as emission of preequilibrium clusters. With an antiproton beam, the annihilation channel constitutes the main mode of interaction [5]. On average five pions are produced per annihilation, which potentially can increase the heating of the residual nucleus.

Experimental studies, consistent with theoretical calculations [6], have already shown that for pions and protons beyond 5 GeV/c, the energy deposition in ^{197}Au-like nuclei saturates [7]. The same saturation phenomenum has been observed at lower energy for a lighter ^{nat}Ag target [8]. This saturation is attributed to the punchthrough of the initial cascade in the target nucleus. In addition, it turns out that the same amount of energy is deposited with both pion and proton beams [7]. In order to enhance the energy deposition with light-ion beams, it is thus necessary to use an antiproton beam.

Studies at LEAR with 200 MeV/c antiprotons, have shown that for $\bar{p}$ annihilation at rest, the mean excitation energy reached in ^{197}Au-like is about 200 MeV, far from the total available energy [9]. Due to the low momentum of the antiproton beam, the annihilation takes place at the surface of the target nucleus, leading to the escape of most of the produced pions. Consequently, one must increase the beam momentum in order to increase the probability for annihilation in the core of the target nucleus. Above 1 GeV/c, the annihilation occurs in flight. Thus, the created pions, benefitting from the trailing motion of the annihilation frame, are emitted forward-focused in the target nucleus. An experiment using 1.9 GeV/c antiprotons at LEAR [10] has shown that the maximum excitation energy measured is about 880 MeV ($\approx$ 5 MeV/A) for ^{197}Au-like nuclei.

The present studies at 8 GeV/c represent the first time that an exclusive measurement has been done with an antiproton beam above 2 GeV/c. Tagged pion and antiproton beams were measured simultaneously during the experiment. Thus, the energy deposition due to the antiproton beam can be directly compared with that of the pion beam.

2 Experimental set-up

The experiment (E900a) was performed with a tagged secondary beam of 8.0 GeV/c negative particles ($\pi^-, K^-, \bar{p}$) at the Brookhaven National Laboratory AGS accelerator. Light-charged particles (LCP=H and He isotopes) and intermediate-mass fragments (IMF: $3 \leq Z < 16$) were measured with the Indiana Silicon Sphere (ISiS) 4π detector array[11]. Beams of $\sim 4 \times 10^6$ particles/cycle (4.5s cycle time and $\approx$ 2.2s spill flattop) were incident on a 2×2 cm^2 self-supporting ^{197}Au target foil of thickness 2 mg/cm^2. To minimize reactions due to beam halo, the target was suspended on two 50 μm tungsten wires. Beam particles were tagged with a time-of-flight/Čerenkov-counter identification system. The time-of-flight system employed a 12 mm-thick Bicron 418 plastic scintillator as a start detector and a 5mm-thick Bicron 418 scintillator 64 m downstream as a stop element. Timing resolution (σ) was $\approx$ 200 ps and provided clean separation of $\bar{p}$ and π^- projectiles (8:1 peak-to-valley ratio). This permitted direct comparison of the $\bar{p}$ and π^- reactions under identical conditions. Beam composition was $\approx$ 98% π^-, 1% K^- and 1% $\bar{p}$ at the target. A

CO_2 Čerenkov counter, operated at atmospheric pressure, was used to identify and veto negative pions that overlapped with the $\bar{p}$ distribution in the time-of-flight spectrum. A segmented halo-veto scintillator array, described in[7], operated in anticoincidence with the TOF-$\check{C}$-ISiS coincidence signals.

The ISiS array consists of 162 gas-ion-chamber/500 μm silicon/28 mm CsI detector telescopes that cover approximately 74% of 4π and polar angles from 14° - 86.5° and 93.5° - 166° [11]. Charged particles with energies $1 \leq E/A \leq 92$ MeV were Z-identified up to $Z \simeq 16$. Isotope resolution was obtained for H, He and Li ejectiles in the energy range $8 \leq E/A \leq 92$ MeV. Also, unidentified fast charged particles (or "gray particles", primarily protons) with energies from 92 to 300 MeV were measured. The minimum-bias ISiS hardware trigger required fast signals in three or more silicon detectors, but did not include "gray particles". The final data set analyzed here contained 24,000 $\bar{p}$ and 2.4 $\times$ 10^6 π^- events in coincidence with one or more He ions or IMFs.

3 Reaction mechanism

In order to have an overview of the reaction mechanism it is interesting to examine the kinematical properties of various emitted products. Fig. 1 shows invariant cross section (velocity) plots of longitudinal (V_{par}/c) versus transverse (V_{per}/c) velocity for Z = 1, 2, 3 and 6 fragments. Note the different velocity scales in each frame. No obvious difference is noticed with these plots between the pion and antiproton beams.

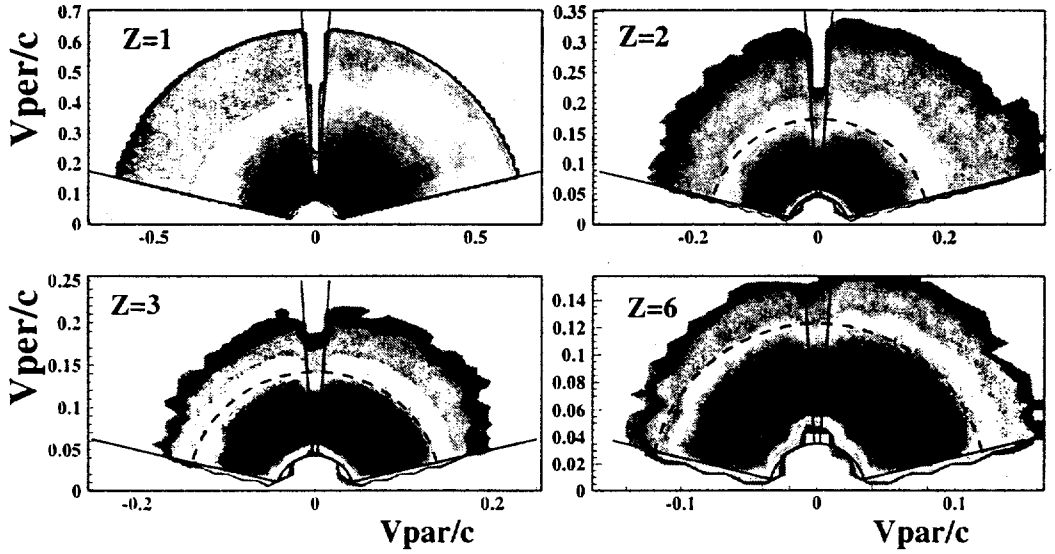

Figure 1: Inclusive invariant cross section plots of longitudinal (V_{par}/c) versus transverse (V_{per}/c) velocity for Z= 1, 2, 3 and 6. The solid lines represent the geometrical limits of ISiS and the dashed lines are the thermal energy cuts defined in text.

For all products with low velocities, one observes an isotropic emission centered near zero source velocity. This slow and isotropic component can be associated with the decay of an equilibrated source with a small recoil velocity. For Z = 1 in Fig. 1, which includes kinetic energies from 3 to 300 MeV, an emission of fast particles forward-focused along the beam axis is apparent. Comparison of the He and Li velocity plots suggests similar nonequilibrium components. These products are likely emitted during the evolution from the initial cascade. For Z=6. which is representative of all Z > 4 IMFs, the forward-focused component is negligible. Indeed, most of the yield of Z > 4 is associated with the slow component. In summary, a thermal-like (slow and isotropic) component and a nonequilibrium (fast and anisotropic) component appear to account for the bulk of the fragments observed in the 8 GeV/c $(\pi^-, \bar{p})+^{197}$Au reactions.

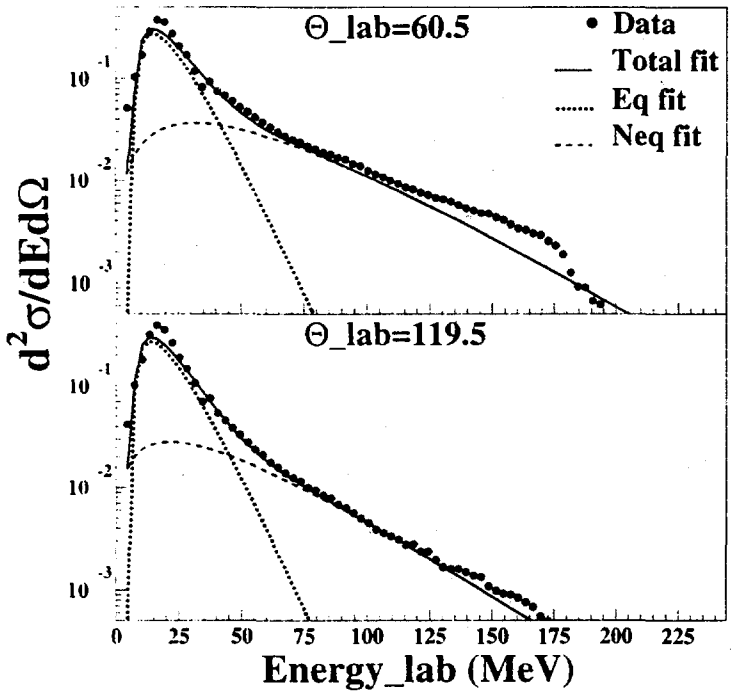

Figure 2: Two-components moving-source fits of the kinetic energy of He ions for a forward (top panel) and its symmetric backward (bottom panel) angle. The global, thermal and nonequilibrium components are, respectively, represented by the plain, dotted and dashed lines. Data correspond to black points.

In order to study the characteristics of the thermal-like residue and determine the amount of deposited energy, it is essential to differentiate between charged particles associated with the fast cascade and those which originate from the thermal-like source. The separation imposed on this analysis is based on a detailed analysis of kinetic energy spectra as a function of total observed charge and IMF multiplicity in the 4.8 GeV ^{3}He + ^{197}Au reaction [8, 12]. Two-component (thermal and nonequilibrium) moving-source fits have been performed over the whole angular range. For the thermal-like component the Moretto formalism [13] has been used in order to reproduce the broad shape of the kinetic energy spectra of heavy IMFs [3]; the preequilibrium component was described with a standard Maxwellian prescription.

Then, based on the calculated fits (see Fig. 2), we define the energy of thermal-like charged particles as protons with kinetic energy K $\leq$ 30 MeV and complex particles with

$$K_i^{CP} < (9.0Z_i + 40)MeV. \quad (1)$$

Nonequilibrium emission corresponds to emitted products with energies greater than the defined cutoff energy. Since the fit of nonequilibrium emission was performed to isolate the thermal component, no statistical interpretation has been made for the Maxwellian description. Representative fits to the spectra are shown in Fig. 2 for He ions for a forward and its symmetric backward angle. One notices that nonequilibrium emission persists in significant yield at the backward angle (at least for Z=1,2).

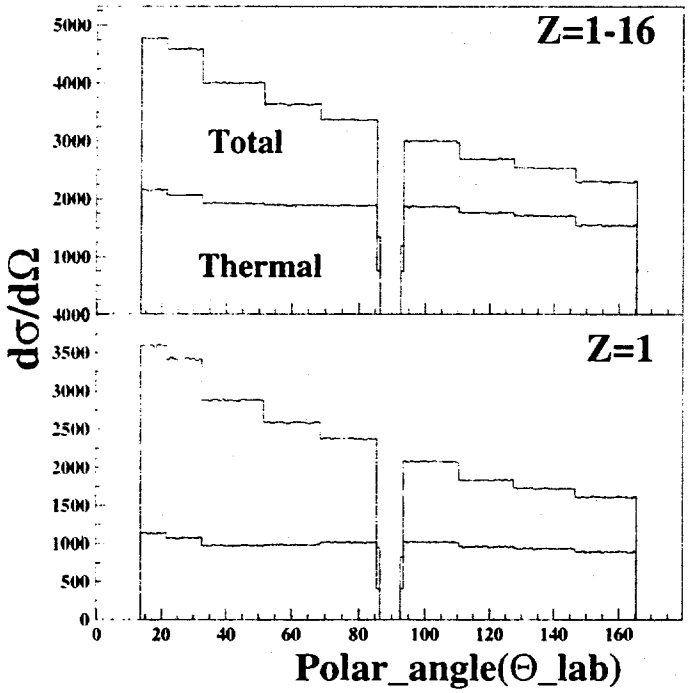

Figure 3: Angular distributions in the laboratory for all emitted products Z=1-16, top panel, and for Z=1, bottom panel. The gray curve corresponds to the thermal component; the white one, to the global component.

In order to check the consistency of this energy cut, we have plotted in Fig. 3 the inclusive angular distributions, as well as that component of the spectra defined as thermal in Eq. (1). The top panel corresponds to all emitted products, the bottom one to Z=1. While the total angular distribution is characteristically forward-peaked (due to the nonequilibrium emission), that for the thermal-like fragments is nearly isotropic. The remaining slight forward focussing of the thermal component can be attributed to the recoil motion of the emitted source ($V_s \sim 0.002c$). The lower panel shows that nonequilibrium emission is mainly due to protons. The high yield of protons (as well as neutrons) at small angles along the beam axis is consistent with the angular distribution of scattering of projectile beams on target nucleons [5]. Based on the integrated yields for the two components, we noted that 55 % of all Z=1 belong to the thermal component, 88 % of Z=2, 97 % of Z=3 more than 99 % of Z $\geq$ 4.

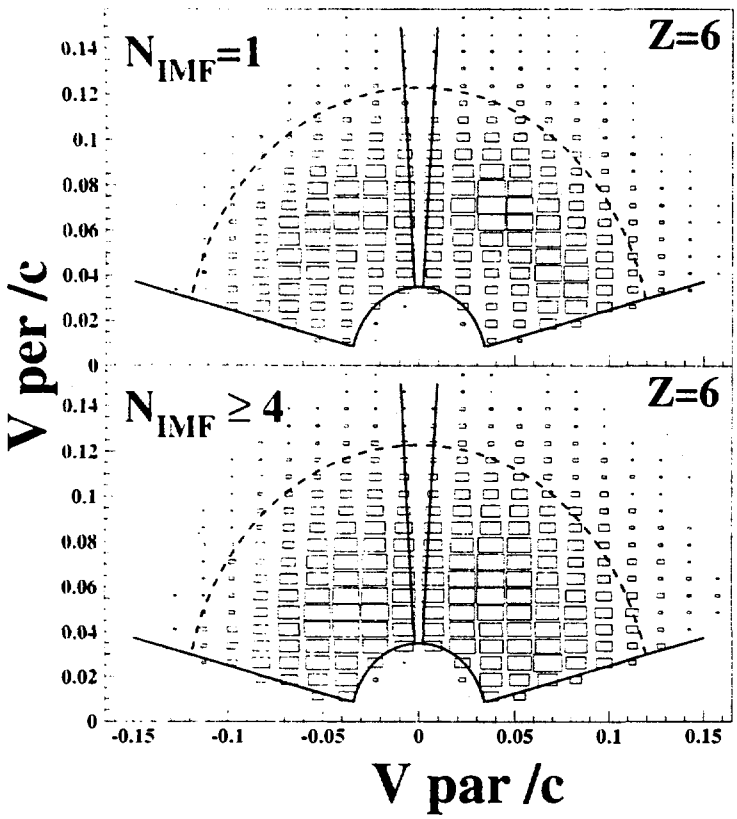

Figure 4: Invariant cross section plots of longitudinal (V_{par}/c) versus transverse (V_{per}/c) velocity for Z= 6 gated on two IMF multiplicity values: $N_{imf} = 1$ and $N_{imf} \geq 4$. The solid lines represent the geometrical limits of ISiS and the dashed lines are the thermal energy cuts defined in text.

Another important feature of the velocity plots is their dependence on IMF multiplicity, related to the excitation energy. In Fig. 3 we show the velocity plots for carbon fragments for two different gates on the observed IMF multiplicity, $N_{IMF} = 1$ and $N_{IMF} \geq 4$. This plot shows that the velocity pattern for the high multiplicity (excitation energy) events is shifted toward lower fragment velocities. Again, this feature of the data is observed for all Z>4 fragments. The shift in the spectra to lower energies cannot be accounted for by source-size arguments alone and may be evidence for thermal expansion of the system [4].

4 Excitation Energy Distributions: $\bar{p}$ vs. π^-

A major objective of experiment E900 was to determine the existence and content of enhanced excitation-energy deposition for $\bar{p}$ beams relative to other hadrons, as predicted by the transport codes. This enhancement is apparent in the charged-particle and IMF multiplicity distributions, as well as in quantities such as the total transverse energy and the total energy of thermalized particles (i.e. those inside dashed lines of Fig. 1)[14].

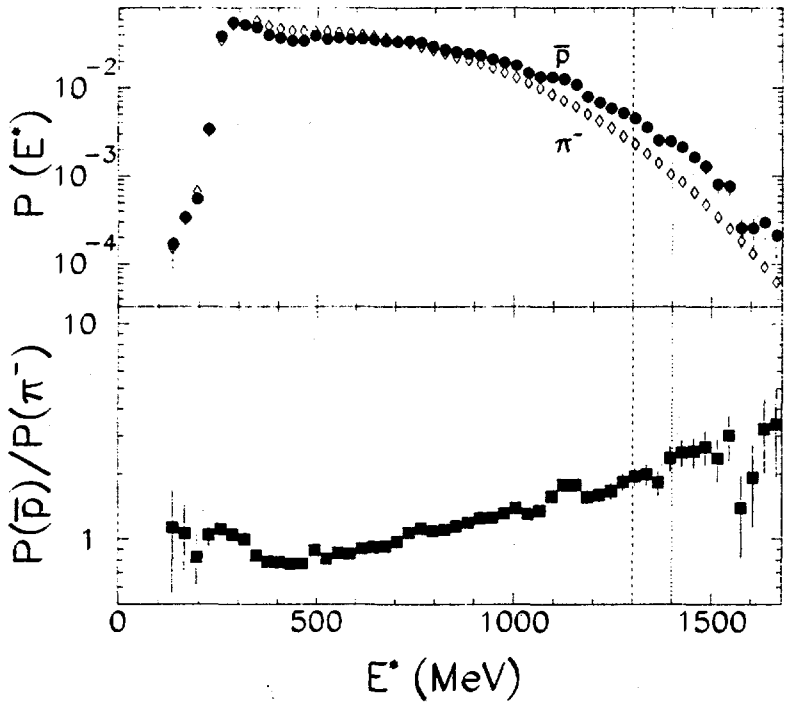

Figure 5: Upper panel: excitation energy probability distributions for reactions of 8 GeV/c π^- (diamonds) and $\bar{p}$ (circles) with ^{197}Au. Lower panel: ratio of excitation energy probability for $\bar{p}$ relative to that for π^-. E* values beyond the vertical dashed lines (dashed π^-; dotted $\bar{p}$) account for 1% of events.

Excitation energies have been determined experimentally on an event-by-event basis according to the prescription,

$$E* = \sum_{i}^{Mc} K_i^{cp} + M_n\langle K_n\rangle + Q + E\gamma. \qquad (2)$$

Here K_i^{CP} is the kinetic energy of each charged-particle detected in an event of charged-particle multiplicity M_c, transformed event-by-event into the source frame. Corrections are also included to account for ISiS geometry. We make two assumptions with regard to the fragment kinetic energy acceptance. The first assumes the thermal energy definition in Eq.(1). The second approach expands the fragment energy acceptance to include a part of the nonequilibrium ejectiles (i.e particles up to E/A $\leq$ 30 MeV/nucleon as performed in [15]).

The second term in Eq.(2) involves the neutron multiplicity, M_n and the average neutron kinetic energy $\langle K_n\rangle$. Measured charged-particle vs. neutron correlations were used to determine M_n [10] and $\langle K_n\rangle$ was initially estimated from Coulomb-corrected proton

spectra and then iterated to obtain a self-consistent value $\langle K_n \rangle = 3/2\ T_{th}$, where $T_{th} = (E^*/a)^{1/2}$ and $a = A/11\ MeV^{-1}$. The reconstructed event serves to define the binding energy difference Q, and the energy released in photons is assumed to be $E\gamma = (M_e + M_n)$ MeV. Both $\bar{p}$ and π^- data were treated identically.

Because of the experimental trigger, the reconstruction procedure is uncertain below $E^* < 250$ MeV, where neutron emission dominates. The charge of the excited residue was obtained by subtracting from the target charge the measured fast charged particles corrected for geometrical acceptance, folded by the corresponding angular distribution. The multiplicity of fast neutrons M_n^{fast} is taken to be $1.93 \times M_p^{fast}$, where M_p^{fast} is the corrected multiplicity of fast protons ($E_p > 30$ MeV). This procedure is intermediate between the experimental systematics of Ref. [9] and the N/Z of the target[16].

In Fig. 5 the top panel shows the reconstructed distribution of excitation energy for the thermal fragment kinetic energy acceptance of Eq. (1). At the 1% cross-section level (vertical lines in Fig. 5), the excitation energy per nucleon is E^*/A =9.0 MeV and 10.3 MeV for π^- and $\bar{p}$ beams, respectively. The excitation-energy enhancement with antiprotons is most apparent when the probability ratio for the two beams is examined, as shown in the bottom frame of Fig. 5. Here it is observed that the probability of reaching the highest excitation energies is at least two times greater for antiprotons than for π^- beam.

With respect to the total available energy in a $\bar{p}$-N collision (4.1 GeV) or a π-Nucleon collision (4 GeV), the fraction of deposited energy is 34 % and 32.5 % for respectively $\bar{p}$ and π beams. These values correspond to the upper 1% of excitation energy distribution (vertical lines in Fig. 5). Thus at least two-thirds of the available energy appears to be taken off by nonequilibrium emission. In addition, we noticed that the mass loss associated with nonequilibrium emission increases with the excitation energy of residues (up to 30 % of the initial mass). In other words, as in heavy-ions collisions [17], it is not possible to heat target nuclei highly without creating a non-negligible component of nonequilibrium emission.

Table 1: Ratio of integrated events beyond multifragmentation threshold ($\sim$ 800-1000 MeV) to events beyond 400 MeV.

Beams	p(GeV/c)	T(GeV)	$\frac{P(E*>800MeV)}{P(E*>400MeV)}$	$\frac{P(E*>1000MeV)}{P(E*>400MeV)}$
$\bar{p}$	8.0	7.1	0.46	0.18
π^-	8.0	7.9	0.36	0.12
^{3}He [17]	7.6	4.8	0.22	0.053
$\bar{p}$ [10]	2.1	1.2	0.068	0.003

Nonetheless, the following comparison indicates that an 8 GeV/c antiproton beam appears the best prescription for heating a ^{197}Au target with hadron beams. In Table 1 the enhanced probability for producing high excitation-energy residues with $\bar{p}$ beams is quantified by comparing with previous measurements involving light-ion projectiles[10, 18].

The comparison shows the fraction of events that exceed the multifragmentation threshold for Au-like residues (E* > 800-1000 MeV [3, 19, 20, 21]), compared to all events with E* > 400 MeV. The integrated results indicate an enhancement of up to 50% for $\bar{p}$ beams relative to π^- in this study and a significantly larger enhancement relative to the 4.8 GeV ^{3}He [18] and 1.22 GeV $\bar{p}$ [10] studies.

5 Comparison with INC calculations

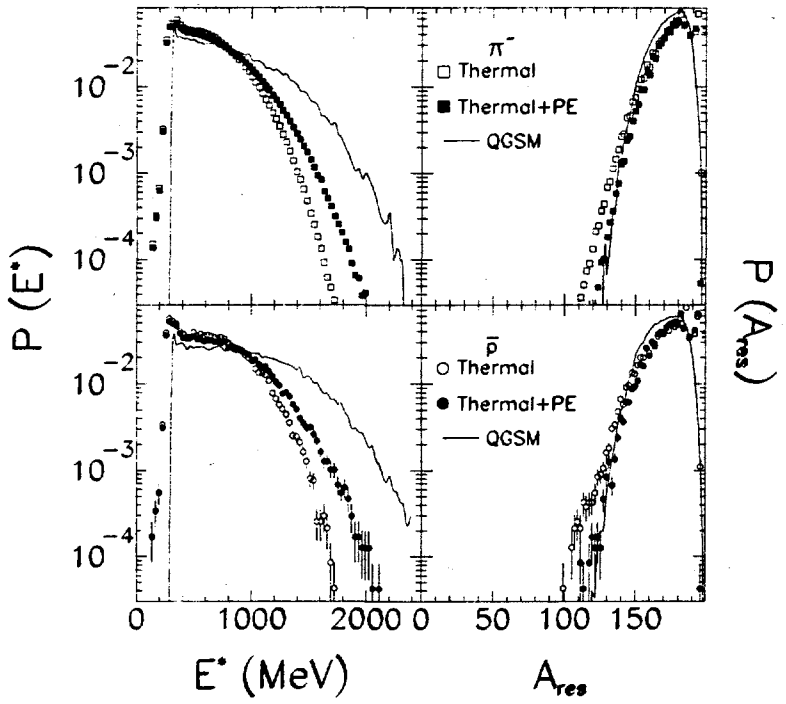

Figure 6: Left: Distribution of excitation energy in target-like residues for π^- (upper) and $\bar{p}$ (lower) beams. Open circles denote thermal particles only; solid circles include all energies up to E/A $\leq$ 30 MeV, and lines give INC prediction [22]. Right: Residue mass distributions; all symbols are the same as for left-hand panels.

In Fig. 6 the data are compared with the prediction of the intranuclear cascade code QGSM of Toneev[22] for the excitation energy distribution of residual nuclei at the end of the fast cascade (30 fm/c). The calculation assumes random impact parameters and the default values of the code, which have been found to reproduce other cascade results at lower beam momenta (< 3 GeV/c). The two left-hand frames compare the experimentally-derived excitation-energy distributions for π^- (top) and $\bar{p}$ (bottom) beams, employing both the thermal protocol of Eq. (1) and that which includes preequilibrium fragments [15]. Although the excitation-energy enhancement with $\bar{p}$ beams is successfully reproduced, the

QGSM prediction overestimates the experimentally-derived excitation energies for both projectiles. On the right, the mass distributions of the excited residues obtained from the event reconstruction procedure is compared with that of the QGSM. The model predicts slightly less mass loss than the data using the thermal assumption, but is in relative accord with that which included preequilibrium emission. The excitation energy and mass comparisons suggest that the probability for pion reabsorption is too high in the code.

6 Conclusions

In summary, we have investigated energy deposition in heavy residues formed in reaction induced by 8 GeV/c π^- and antiproton beams. After removing the nonequilibrium component, the characteristics of the thermal-like component are consistent with those of an equilibrated source. Event reconstruction of the residue mass and excitation energy distributions confirm that the probability for reaching high excitation energies is significantly enhanced in antiproton reactions at this beam momentum. The INC predictions using the QGSM model are qualitatively in agreement with the experimental results, but overestimate the absolute excitation energy values for both projectiles.

References

[1] G.Wang, K. Kwiatkowski, V.E. Viola, W. Bauer and P. Danielewicz, Phys. Rev. C **53**, 1811 (1996).

[2] J. Cugnon, *et al.*, Nucl. Phys. **A470**, 558 (1987), Phys. of At. Nucl. **57**, 1075 (1994).

[3] K. Kwiatkowski *et al.*, Phys. Rev. Lett. **74**, 3756 (1995).

[4] G.Wang, *et al.*, Phys. Lett. B **393**, 290 (1997).

[5] Ye.S. Golubeva, Nuc. Phys. A **483**, 539 (1988).

[6] L. Beaulieu *et al.* in *Proceedings of the Winter Workshop on Nuclear Dynamics, Park City, UT, 1999* to be published; D.S. Ginger, Senior Honors Thesis, Indiana University, 1997.

[7] W-c. Hsi, *et al.*, Phys. Rev. Lett.**79**, 817 (1997).

[8] K.B. Morley *et al.*, Phys. Rev. C. **54**, 737 (1996).

[9] D. Polster *et al.* Phys. Rev. C **51**, 1167 (1995).

[10] F. Goldenbaum *et al.*, Phys. Rev. Lett. **77** 1230, (1996); L. Pienkowski *et al.*, Phys. Lett B **336**, 147, (1994).

[11] K. Kwiatkowski *et al.*, Nucl. Instr. Meth. **A360**, 571 (1995).

[12] D.S. Bracken, Ph.D. thesis, Indiana University, 1996.

[13] L.G. Moretto, *et al.*, Nuc. Phys. A **247**, 211 (1975).

[14] T. Lefort *et al.*, submitted to Phys. Rev. Lett.

[15] J.A. Hauger, *et al.*, Phys. Rev. Lett. **77**, 235 (1996).

[16] I.A.Pshenichnov *et al.*, Phys. Rev. C **52**, 947 (1995).

[17] D. Cussol *et al.*, D. Doré *et al*, Proc. XXXVIth Int. Winter Meeting on Nuc. Phys., ed by I. Iori, Bormio Italy, (January 1998).

[18] K. Kwiatkowski *et al.*, Phys. Lett.**B 423**, 21 (1998).

[19] W.A. Friedman, Phys. Rev. C **42**, 667 (1990).

[20] J. Bondorf. *et al.*, Nucl. Phys. **A443**, 221 (1985).

[21] D.H.E. Gross, Rep. Prog. Phys. **53** 605 (1990).

[22] V. Toneev, N.S. Amelin, K.K. Gudima and S. Yu. Sivoklokov, Nucl. Phys. **A519**, 463 (1990).